Oxygen-vacancy ordering in lanthanide-doped ceria: Dopant-type dependence and structure model

Ding Rong Ou,[1,*] Toshiyuki Mori,[1] Fei Ye,[1] Jin Zou,[2,3] Graeme Auchterlonie,[3] and John Drennan[3]

[1]*Fuel Cell Materials Center, National Institute for Materials Science, 1-1 Namiki, Tsukuba, Ibaraki 305-0044, Japan*
[2]*School of Engineering, The University of Queensland, St. Lucia, Queensland 4072, Australia*
[3]*Centre for Microscopy and Microanalysis, The University of Queensland, St. Lucia, Queensland 4072, Australia*

Studies of electron energy loss spectroscopy and selected area electron diffraction (SAED) were systematically performed on 15 and 25 at. % lanthanide (Ln)-doped ceria samples (Ln=Sm, Gd, Dy, and Yb), through which the local ordering of oxygen vacancies that develops with increase in doping level was confirmed in the sequence of $(Gd, Sm) > Dy > Yb$. Furthermore, a monotone correlation between the development of the ordering and the degradation of ionic conductivity with increasing the doping concentration from 15 to 25 at. % was observed. Based on the analysis of SAED patterns, a structural model for the ordering of oxygen vacancies has been constructed, in which the arrangement of oxygen vacancies is similar to that in C-type Ln_2O_3 oxides and the $\frac{1}{2}\langle 110 \rangle$ pairs of the vacancies are preferred. Then, the factors that can influence the formation of the ordering are discussed.

PACS number(s): 61.72.$-$y, 61.05.J$-$, 66.10.Ed, 82.45.Gj

I. INTRODUCTION

As a promising ionic conductor that can be used as electrolytic materials in the intermediate-temperature solid oxide fuel cells (SOFCs), rare-earth-doped ceria with cubic fluorite structure has attracted increasing attentions in recent years.[1–4] Many studies have demonstrated that the electrical properties of doped ceria can be significantly influenced by the dopant type.[2–4] There exists an *optimum radius* of the dopant for ionic conduction. As the dopant radius deviates from this optimum value, the ionic conductivity of doped ceria decreases dramatically. This phenomenon has been attributed to the dopant-oxygen vacancy association that depends on the dopant radius.[2,5–7] In the dilute doping range, the ionic conduction is dominated by this association and exhibits a maximum conductivity for ceria doped with Sm or Gd because these dopant cations have the optimum radius, and thereby have a smaller association enthalpy.[2–4] However, in heavily doped ceria, nanosized domains can form and give negative impacts on the ionic conduction.[8–11] These domains have higher dopant concentrations than the matrix and could provide deep traps for the oxygen vacancies.[10,12] As a result of the domain formation, the advantage of the dopant having an optimum radius disappears with increasing the doping level. As shown in a comparative study of Gd- and Y-doped ceria,[13] conductivities in the order of $Gd > Y$ and $Gd < Y$ were observed, respectively, at doping concentrations lower and higher than 20–25 at. %. Zhang *et al.*[13] suggested that this occurs because the ionic conduction in heavily doped ceria is dominated by the formation of nanosized domains, instead of being dominated by the dopant-oxygen vacancy association.

Because of the small size, the immature structure, and the lattice coherence with the fluorite-structured matrix,[10,11] the direct analysis on these domains is difficult and their crystal structure remains unclear. Despite this, it has been suspected that the negative impacts of domains on ionic conduction are partly related to its ordered structure, which may involve the local ordering of oxygen vacancies.[11–13] In cubic stabilized zirconia, a more familiar system, the local ordering of oxygen vacancies was also speculated, which has ordered structures depending on the composition (e.g., the dopant type and doping concentration) and the heat treatment.[14–16] Based on the study of x-ray diffraction, Welberry *et al.* suggested that the local ordering in yttria-stabilized zirconia has a pyrochlorelike structure, in which the $\frac{1}{2}\langle 111 \rangle$ pairs of oxygen vacancies across cubes of oxygen anions containing the cations are allowed.[14] In addition, the "δ phase" and the C-type oxide were also suggested in some stabilized zirconia based on the study of selected area electron diffraction (SAED).[15,16] In our previous work,[17] the local ordering of oxygen vacancies in some heavily rare-earth-doped ceria samples has been demonstrated by the study of electron energy loss spectroscopy (EELS), which could be affected by dopant type and may partly contribute to the dopant-type dependence of electrical properties of these heavily doped samples. Based on SAED patterns with [110] axis, a C-type-related structure was suspected for the ordering.[17] However, the confirmation of this structure is required and the detailed structure model, e.g., the manner of the vacancy arrangement and of the dopant-vacancy association, is still unclear.

Therefore, further studies on the inhomogeneous microstructures in doped ceria, e.g., the nanosized domains and the oxygen-vacancy ordering, are desired to understand their development and influence mechanisms, which are of importance to the control of microstructure at nanoscale and the design of high-quality electrolytes for intermediate-temperature SOFCs. In this paper, the emphasis is laid on the local ordering of oxygen vacancies in lanthanide (Ln)-doped ceria. To detailedly characterize the oxygen-vacancy ordering, systematic studies of EELS and SAED were performed on 15 and 25 at. % Ln-doped ceria because EELS may be used to detect the oxygen-vacancy ordering in nonstoichiometric oxides[17–19] and SAED may provide the structural information of the ordering. Compared with the previous work,[17] clearer relationships of the oxygen-vacancy ordering,

the doping level, the dopant type, and the electrical conductivity are obtained from these studies. Then, a detailed structural model and a mechanism for the development of oxygen-vacancy ordering in Ln-doped ceria are proposed.

II. EXPERIMENT

Spherical-shaped and well-dispersed nanopowders of 15 and 25 at. % Ln-doped ceria (Ln=Sm, Gd, Dy and Yb) were synthesized by the ammonium carbonate coprecipitation method[11] using cerium and Ln nitrate hydrates as cation sources and ammonium carbonate as precipitant. The reaction temperature is between 60 and 70 °C. After the entire mix was aged for 1 h at the reaction temperature, the precipitates were collected by suction filtering, washed by distilled water and ethanol, and finally dried at the room temperature under the flowing nitrogen. By calcining the dried precipitates at 700–800 °C for 2 h in oxygen environment, fine oxide powders were obtained. The analysis by scanning electron microscope (SEM, HITACHI S-5000) showed that the particle size of resultant oxides is about 20–40 nm. Then, highly dense bulk samples were obtained from the nanopowders, through sintering at 1400–1450 °C for 6 h. The average grain size of sintered samples was determined by SEM observation and by linear intercept method,[20] whose value is about 0.8–1 μm for all samples.

Detailed microstructural features of the samples were examined by transmission electron microscope (TEM). To prepare specimens for TEM observation, small disks with a diameter of 3 mm were cut from the central region of the sintered samples. The thickness of the disks was reduced by mechanical polishing and dimpling, followed by ion milling. SAED and EELS studies were performed, respectively, in a JEOL JEM-2000EX TEM and in a FEI Tecnai-F30 TEM equipped with a Gatan imaging filtering system. The aperture size for SAED is about 0.2 μm on TEM images. The regions selected for EELS study were deviated from the strong Bragg reflections and chosen to be with a thickness of 0.1–0.2 inelastic mean free paths (about 10–20 nm). To avoid the influence of irradiation damage,[21] a spread beam and a short acquirement time no longer than 5 s were applied. The power-law technique[22] was used to subtract the background.

The electrical conductivities of sintered samples were measured in air by a three-probe dc measurement. Before the measurement, the disk-shaped samples with a diameter of about 10 mm were painted with platinum paste on both sides and fired at 1000 °C for 1 h to ensure a good thermal and electrical bond between the sample surfaces and the platinum electrodes. The measurement was performed after the temperature was held at the designed level for 1 h for the thermal stabilization.

For the purpose of comparison with Ln-doped ceria which will be given in Sec. V, 15 and 25 at. % Y-doped ceria samples were also prepared and characterized using the aforementioned experimental procedures.

III. EXPERIMENTAL RESULTS

A. Dopant-type dependence of oxygen-vacancy ordering

Figure 1 shows the typical spectra of oxygen K edge of 15 and 25 at. % Ln-doped ceria samples after subtracting the
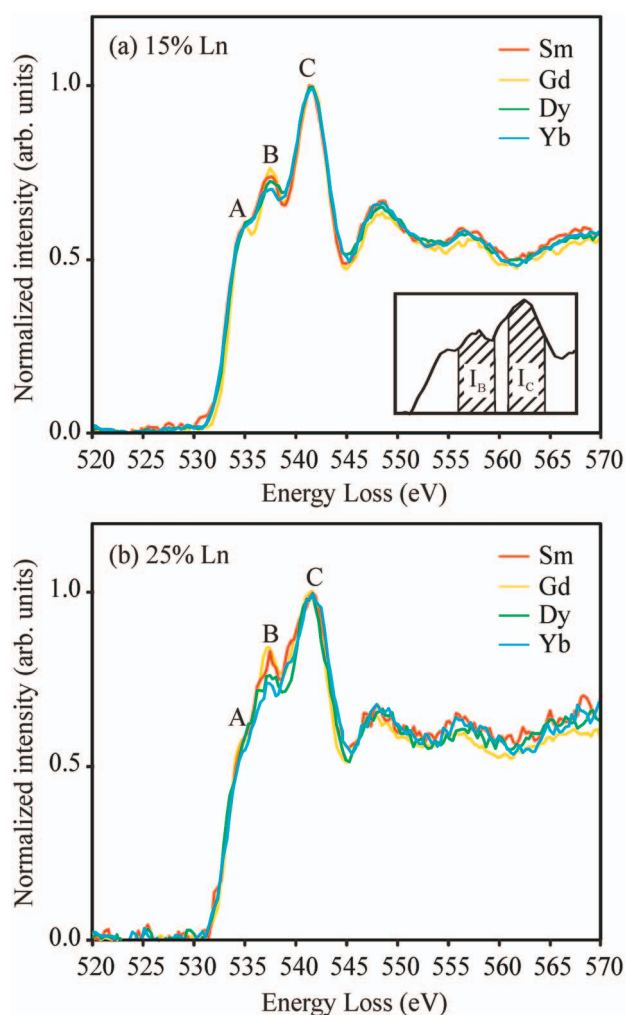

FIG. 1. (Color) Oxygen K edge of (a) 15 and (b) 25 at. % Ln-doped ceria samples. The spectra were normalized with respect to the intensity of peak C. Inset shows the energy windows with a width of 2 eV for calculating the integral intensities of peaks B and C.

background. Three main features labeled by A, B, and C are observed above the threshold. Among these features, the small shoulder marked by A can be attributed to the transition $O1s \rightarrow O2p$ hybridized with f-character states of Ce^{4+} cations in Ln-doped ceria.[23,24] It is stronger in the 15 at. % Ln-doped ceria because of the higher Ce concentration in these samples. The intense peaks B and C can be interpreted as transitions toward O $2p$ state hybridized with Ce (or dopant) $5d$-e_g and $5d$-t_{2g} states that are split under the crystal-field effects.[25,26] Therefore, the relative intensity of peaks B and C is sensitive to the change in crystal structure. Particularly, in nonstoichiometric oxides, it has been suggested that the enhancement of peak B could be introduced by the local ordering of oxygen vacancies.[17,18] For the purpose of quantitative comparison, the integral intensities of peaks B and C (I_B and I_C) were calculated using an energy window of 2 eV open on the peaks [as illustrated in the inset of Fig. 1(a)] and the relative intensity of peak B was calculated as I_B/I_C. Thus, a larger value of I_B/I_C indicates a higher degree of the local ordering in Ln-doped ceria samples. As can be seen from
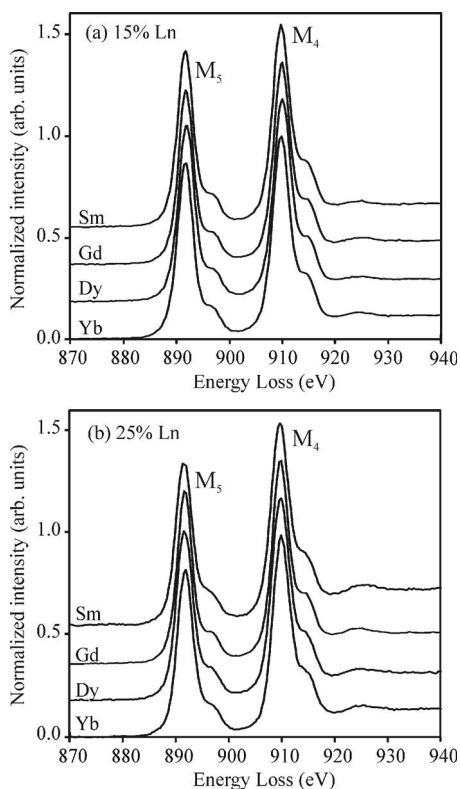
FIG. 2. Ce $M_{4,5}$ edge of (a) 15 and (b) 25 at. % Ln-doped ceria samples. The spectra were normalized with respect to the intensity of peak M_4.

Fig. 1, the local ordering of oxygen vacancies depends on both the doping level and the dopant type. For 15 at. % Ln-doped ceria [Fig. 1(a)], the calculated values of I_B/I_C are about 0.73–0.75, with slightly higher values observed in Sm- and Gd-doped ceria. As the doping concentration increases to 25 at. % [Fig. 1(b)], I_B/I_C increases to about 0.75–0.81 and a sequence of $(Gd, Sm) > Dy > Yb$ is readily seen. These results indicate that the oxygen vacancy ordering could develop in Ln-doped ceria with increasing the doping level and a higher degree of the ordering tends to form in Sm- and Gd-doped ceria regardless of the doping concentration, 15 or 25 at. %.

Figure 2 shows the Ce $M_{4,5}$ edge of 15 and 25 at. % Ln-doped ceria samples. The ratio of I_{M_4}/I_{M_5}, where I_{M_4} and I_{M_5} are peak values on the $M_{4,5}$ edge, is about 1.2 for all spectra, showing that Ce exists predominantly as a tetravalent ion.[27,28] Thus, the effect of irradiation-induced reduction, which may cause increase in trivalent Ce,[21] can be ignored. Since the content of trivalent Ce is negligible, it can be concluded that the concentration of oxygen vacancy is determined by the doping level and the oxygen-vacancy ordering revealed by EELS is mainly due to the influence of the dopant.

It has been reported that the oxygen-vacancy ordering may have negative impacts on the ionic conduction in heavily doped ceria.[17] In this work, the EELS study of oxygen-vacancy ordering was performed at room temperature, while the operating temperature of SOFCs based on doped ceria electrolyte, and thereby the measurement tem-

TABLE I. Ionic conductivity (in air) of 15 and 25 at. % Ln-doped ceria (σ_{15} and σ_{25}).

Dopant	Ionic conductivity at 500 °C (S/cm)		
	$\log \sigma_{15}$	$\log \sigma_{25}$	$\log \sigma_{15} - \log \sigma_{25}$
Sm	−2.28	−2.89	0.61
Gd	−2.41	−3.19	0.78
Dy	−2.42	−2.78	0.36
Yb	−2.74	−2.93	0.19

perature for the ionic conduction in doped ceria, is around 500 °C. Nevertheless, the segregation of the dopant[10,12] and the local ordering of oxygen vacancies may also exist at the measurement temperature ($\sim$500 °C) and have influence on the electrical conductivity because the microstructural rearrangement in doped ceria is difficult at temperatures much lower than 1000 °C.[29] To quantitatively clarify the impacts of the ordering on ionic conduction and its dependences on dopant type and doping level, the development of oxygen-vacancy ordering with increasing doping level was estimated by the enhancement of peak B and calculated as $\Delta(I_B/I_C)_{25-15} = (I_B/I_C)_{25} - (I_B/I_C)_{15}$, where the subscripts 15 and 25 indicate the doping concentration. The conductivities of 15 and 25 at. % Ln-doped ceria samples measured at 500 °C are listed in Table I, in which the data of Sm-, Dy- and Yb-doped ceria are the same as those reported in Ref. 17. In all these Ln-doped ceria samples, the electrical conduction is predominantly ionic in air at intermediate temperature (around 500 °C).[2–4] As the doping concentration increases from 15 to 25 at. %, a dramatic decrease in the conductivity was observed, as listed in Table I. Though the measured conductivity includes contributions of both the grain boundaries and the bulk, it is believed that the decrease in conductivity is mainly due to the change in bulk conductivity because the grain size, and thereby the density of grain boundary, is similar in different samples. Specifically, as suggested in previous studies,[8–12] this decrease can be explained by the enhanced interaction between the oxygen vacancies and the segregated dopant cations in some regions named microdomains or nanosized domains. In addition, the oxygen-vacancy ordering may also affect the ionic conductivity. In 15 at. % Ln-doped ceria, the ordering is not strong enough and the conductivity is still dominated by the simple dopant-vacancy association, which can be evidenced by the higher conductivity observed in Sm- and Gd-doped ceria. In 25 at. % Ln-doped ceria, the advantage of Sm- and Gd-doped ceria disappears and then a greater decrease in conductivity with increasing the doping level was observed in Sm- and Gd-doped ceria, which agrees with the higher degree of oxygen-vacancy ordering in these samples. Figure 3 clearly shows a monotone correlation between $\Delta(I_B/I_C)_{25-15}$ and the degradation of electrical conductivity. It indicates that, in addition to the interaction between the oxygen vacancies and segregated dopant cations, the mobility of the oxygen vacancies can be further decreased by the ordering of oxygen vacancies and a higher degree of the ordering can block the migration of vacancies more effectively.
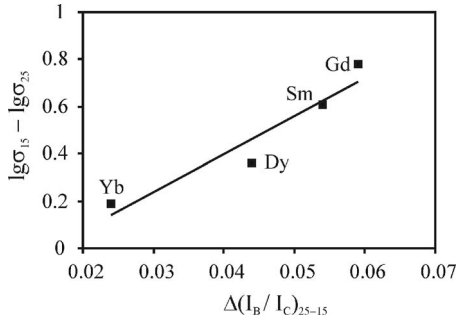
FIG. 3. Correlation between the value of $\Delta(I_B/I_C)_{25-15}$ of Ln-doped ceria and the decrease in conductivity with increasing doping concentration from 15 to 25 at. %.

B. Structural analysis of the ordering

To further understand the structural feature of the oxygen-vacancy ordering, SAED study was carried out. Figure 4 displays [110] SAED patterns recorded from 15 and 25 at. % Ln-doped ceria samples. On the patterns of 15 at. % Ln-doped ceria samples, weak diffuse scatterings imposed on the diffraction pattern of fluorite structure are observed, while on those of 25 at. % Ln-doped ceria samples, the diffuse scatterings are enhanced and the extra reflections can be noticed. In investigations of ceria-based oxides, it has been demonstrated that the difference between SAED patterns of 15 and 25 at. % Ln-doped ceria samples is mainly due to the change in the density of microstructural inhomogeneity, which is dilute in 15 at. % Ln-doped ceria but becomes dense as the doping concentration is 25 at. %.[10,11] Furthermore, brighter diffuse scatterings and clearer extra reflections likely appear on the patterns of Sm- and Gd-doped ceria. Though the contrast in SAED patterns could be influenced by sample thickness and exposure time, one can find a good consistence between the development of diffuse scatterings and extra reflections and the increase in oxygen-vacancy ordering revealed by the EELS study. It indicates that the formation of local ordering of oxygen vacancies in the fluorite-structured matrix can contribute to the aforementioned additional features on SAED patterns, especially to the extra reflections.

Figure 5 displays [100], [111], and [112] SAED patterns of 25 at. % Gd-doped ceria, on which both diffuse scatterings and extra reflections can be readily seen. These features can be also seen on the patterns of other doped ceria while their intensity presents a dependence on dopant type and doping concentration, as shown in Fig. 4. Since the contours of the diffuse scatterings and the distribution of extra reflections are similar in samples doped with different Ln elements and having various doping concentrations, it is reasonable to suggest that the local ordering in doped ceria could have some common structures. Especially, the extra reflections located at the crossing points of diffuse scatterings may indicate a more mature status of the ordering. Hence, based on the SAED patterns, the three-dimensional distributions of the extra reflections and diffuse scatterings in a unit cell in reciprocal space are constructed for doped ceria. As shown in Fig. 6(a), the 12 satellite extra reflections around a reflection of fluorite structure can be described as $G_F + \frac{1}{4}\{220\}^*$, where G_F is a reciprocal lattice vector of the fluorite structure. Because no extra reflections were observed on [100] SAED patterns, it is suggested that the satellite reflections are only located around the $(111)^*$ reflection and those around the $(000)^*$ and equivalent reflections on the [110], [111], and [112] patterns are due to double diffraction occurring as the electron beam passes through the matrix and the ordered structure. In Fig. 6(b), the distribution of diffuse scatterings is composed of eight cylindroids with their rotational axes parallel to the $\langle 111 \rangle$ directions of the bcc reciprocal lattice. The diffuse scatterings are assumed to be distributed on the cylindroid surfaces. As illustrated in Fig. 6(b), the arc for building the rotational cylindroids is a part of the circle with
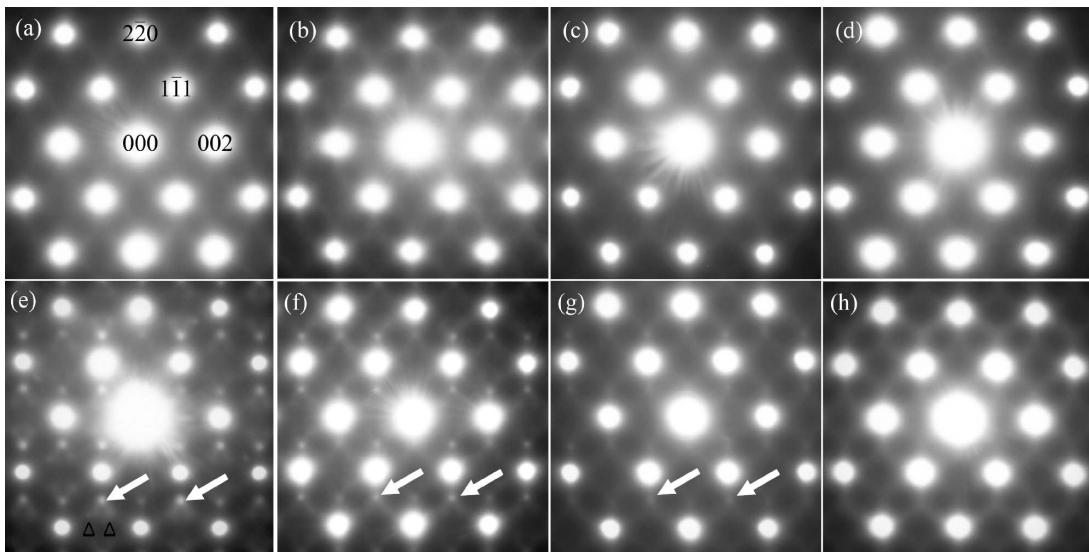

FIG. 4. [110] SAED patterns of [(a)–(d)] 15 at. % and [(e)–(h)] 25 at. % Ln-doped ceria samples; from left to right: Ln=Sm, Gd, Dy, and Yb. Arrows and triangles indicate the satellite reflections of $G_F + \frac{1}{4}\{220\}^*$ and $G_F + \frac{1}{4}\{311\}^*$, respectively.
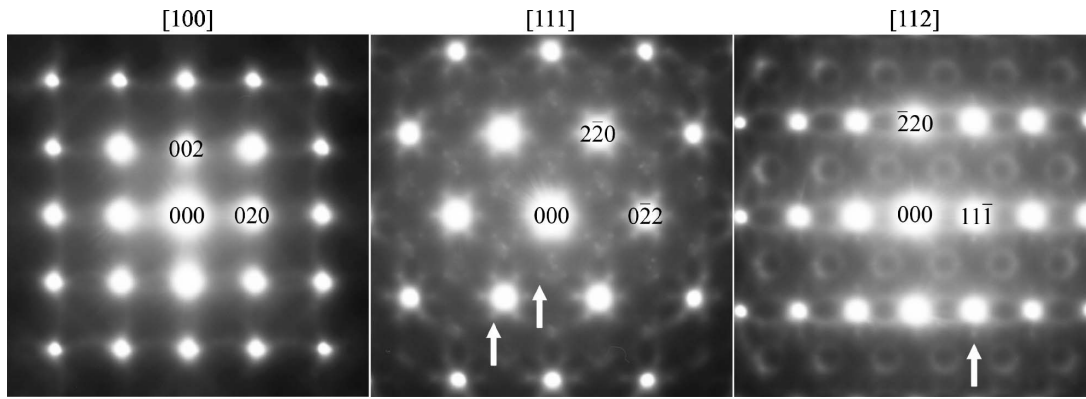
FIG. 5. [100], [111], and [112] SAED patterns of 25 at. % Gd-doped ceria.

the center at the point of $\frac{3}{4}(011)^*$ and crossing the reflections of $(000)^*$ and $(111)^*$. To fit in with the SAED patterns, the overlaps between the cylindroids are adjusted as small planes [as one indicated in Fig. 6(b)]. In Fig. 7, two-dimensional (2D) cross sections of this three-dimensional (3D) model are given, on which the distributions of the diffuse scatterings and the satellite extra reflections located at crossing points of the cylindroids are in good agreement with the main features of the SAED patterns in Figs. 4 and 5.

In addition to the diffuse scatterings and extra reflections illustrated in Fig. 6, other weak features were also observed in SAED patterns of Sm- and Gd-doped ceria samples, e.g., the weak diffuse scatterings with their rotational axes parallel to the $\langle 200 \rangle$ directions of the bcc reciprocal lattice [Fig. 5(a)] and very dim extra reflections located at some of the $G_F + \frac{1}{4}\{311\}^*$ positions [as marked by triangles in Fig. 4(e)]. It is

possible that there exist more than one type of local ordering in the sample and the weak features correspond to a minor one. However, these weaker features cannot be consistently observed on SAED patterns in different zones and, thereby, their distribution in reciprocal space remains unclear.

IV. STRUCTURAL MODEL OF THE OXYGEN-VACANCY ORDERING

The analysis of distributions of diffuse scatterings and extra reflections indicates that the ordering of oxygen vacancies in doped ceria has a cubic structure with symmetry similar to the matrix, which is probably a superstructure based on the fluorite structure. Since a solid solution of Ce in C-type Ln_2O_3 can form in CeO_2-$LnO_{1.5}$ systems at higher doping concentrations ($>33\%-40\%$),[30,31] the oxygen-vacancy ordering that appears before the formation of C-type Ln_2O_3 could be a symptom of a transition from the fluorite ceria to the C-type Ln_2O_3 and have a C-type-related structure. As shown in Fig. 8(a), a unit cell of the C-type structure of Ln_2O_3 can be constructed out of eight unit cells of fluorite structure by removing 25% of oxygen ions with introducing
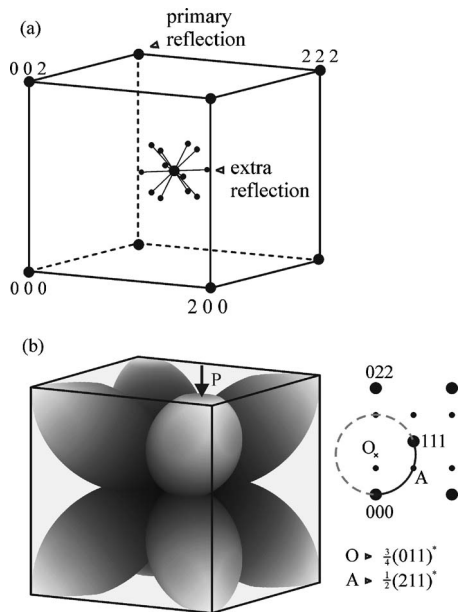

FIG. 6. Three-dimensional distribution of (a) the extra reflections and (b) the diffuse scatterings in a unit cell in reciprocal space, with the letter P indicating one of small planes caused by the overlap of cylindroids. The arc for building the cylindroids is illustrated in (b).
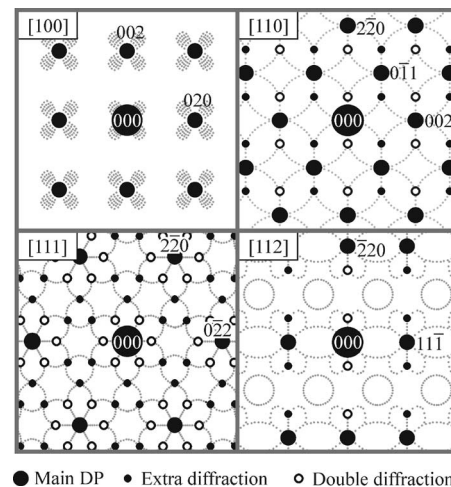

FIG. 7. The 2D cross sections of 3D distribution in Fig. 6, with view directions along [100], [110], [111], and [112]. The small gray dots indicate the contours of the diffuse scatterings.
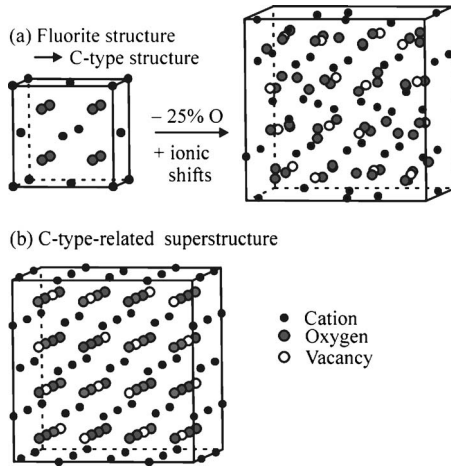
FIG. 8. (a) Schematic of constructing a unit cell of C-type structure of Ln_2O_3 out of eight unit cells of fluorite structure by removing 25% oxygen ions with introducing ionic shifts. (b) C-type-related superstructure of the oxygen-vacancy ordering.

atomic shifts. Due to the high lattice stability of metal oxide and the small size of the local ordering, we ignore the atomic displacement and suspect that the superstructure for the local ordering has the arrangement of vacancies as in the C-type structure but the atomic positions remain as in the fluorite structure [Fig. 8(b)]. This superstructure can be described in the cubic space group $Ia\bar{3}$ (No. 206) as the C-type structure, with the oxygen vacancies located at the $16c$ sites (see Table II). Simulations using the software CARINE CRYSTALLOGRA-PHY v3.1 show that the resultant diffraction pattern of the suggested superstructure consists of strong reflections similar to those of fluorite structure and satellite reflections located at 12 $G_F + \frac{1}{4}\{220\}^*$ positions around the $(111)^*$ reflection of the bcc reciprocal unit cell, which agrees well with the experimental results shown in Fig. 6(a).

However, in practical materials, the local concentration of oxygen vacancies in doped ceria is usually less than that shown in Fig. 8(b), and the $16c$ sites could be occupied with the mixture of oxygen anions and vacancies. In this case, the local ordering could appear with looser distribution of the vacancies, e.g., chains and networks based on the superstruc-
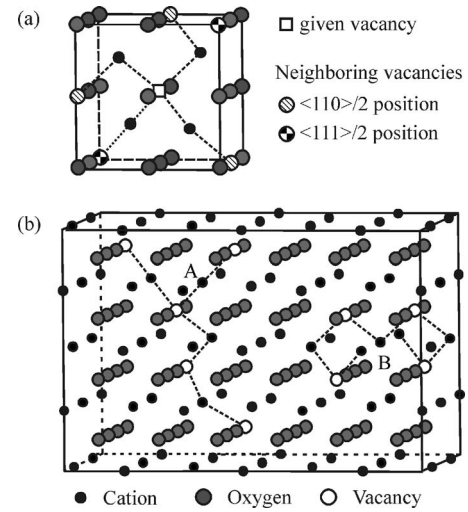

FIG. 9. (a) The atomic environment around a given oxygen vacancy in the superstructure; (b) the possible structure of oxygen vacancies in practical materials: A, irregular chains and networks; B, helical chains.

ture. As shown in Fig. 9(a), around an oxygen vacancy in the suggested superstructure, there could be three $\frac{1}{2}\langle 110 \rangle$ and one $\frac{1}{2}\langle 111 \rangle$ vacancy connections containing the cations. With these basic connections, helical chains, irregular chains, and networks of the vacancies can be formed, as illustrated in Fig. 9(b). Figure 9(a) also shows a possible $\frac{1}{2}\langle 111 \rangle$ connection that crosses the cube of oxygen anions without a cation; however, we suspect that such direct connection without an intermediate cation is probably less stable because of the strong Coulomb repulsion between the vacancies, and thereby rarely appears unless in a dense distribution of oxygen vacancies.

By comparing the structure model of local ordering of oxygen vacancies in doped ceria and in stabilized zirconia, one can find an interesting correlation between the basic connections of oxygen vacancies and the resultant ordered structure. In stabilized zirconia, the connections of vacancies most likely form $\frac{1}{2}\langle 111 \rangle$ pairs across cubes of oxygen anions containing the cations and tend to result in a pyrochlorelike structure,[14,15] while the $\frac{1}{2}\langle 110 \rangle$ pairs and C-type-related su-

TABLE II. Description of the C-type structure and the superstructure of oxygen-vacancy ordering in the cubic space group $Ia\bar{3}$.

Structure type	Space group	Atoms	Wyckoff notation	x	y	z
C-type structure	$Ia\bar{3}$ (No. 206)	Cation	$8b$	0.25	0.25	0.25
		Cation	$24d$	$\delta_1{}^a$	0	0.25
		Oxygen	$48e$	$0.375 + \delta_2{}^a$	$0.125 + \delta_3{}^a$	$0.375 + \delta_4{}^a$
Superstructure	$Ia\bar{3}$ (No. 206)	Cation	$8b$	0.25	0.25	0.25
		Cation	$24d$	0	0	0.25
		Oxygen	$48e$	0.375	0.125	0.375
		Vacancy	$16c$	0.375	0.375	0.375

$^a\delta_i$ ($i = 1-4$): the atomic displacements in C-type Ln_2O_3 compared with the suggested superstructure.

perstructure are more preferred in doped ceria. For this reason, we believe that the relative thermal stability of the oxygen-vacancy connections could be a key factor to determine the possible structure of the ordering, which can be influenced by the dopant type, the doping concentration, and the surrounding matrix.

V. DISCUSSION

Recent studies revealed that, in practical materials of doped ceria, the microstructure can be complicated. Besides clusters of defects, the development of nanosized domains with increasing doping level was reported in doped ceria.[8–11] It has been demonstrated that diffuse scatterings and extra reflections on SAED patterns can be attributed to the formation of these domains. Furthermore, the studies of energy-filtering TEM (EFTEM) and high-angle annular dark-field scanning TEM (HAADF-STEM) have separately shown that these domains have higher dopant concentration than their matrix.[10,12] In addition to these microstructural features, oxygen-vacancy ordering was further confirmed[17] and the relationship between the ordering and the doping concentration is clearly shown in this study.

Since the oxygen vacancies can be associated with dopant cations due to the requirement of electrical neutrality, we believe that the ordering of oxygen vacancies determined in this study is primarily localized in and around the domains of higher dopant concentration and that the segregation of oxygen vacancies with the dopant cations plays an important role in the ordering. The importance of the segregation can be explained as follows. In a fluorite structure, there are 26 neighboring oxygen sites around an oxygen vacancy, including 6 in $\frac{1}{2}\langle 100 \rangle$ sites (the nearest-neighboring sites), 12 in $\frac{1}{2}\langle 110 \rangle$ sites (the second-neighboring sites), and 8 in $\frac{1}{2}\langle 111 \rangle$ sites (the third-neighboring sites). Within these sites, pairs of oxygen vacancies probably form.[14] Thus, the possible number of neighboring oxygen vacancies (P_{VO}) that could be connected with the given vacancy can be approximately estimated by $P_{VO}=27 n_v - 1$ and $n_v = x/4$, where n_v is the vacancy concentration on oxygen sites and x is the dopant concentration. If we ignore the segregation of dopant cations and oxygen vacancies, the value of P_{VO} is about 0.7 at a doping concentration of 25 at. % ($x=0.25$), which possibly enables the formation of oxygen-vacancy pairs and triples but limits the formation of chains and other ordered structures. In contrast, with considering the segregation of dopant cations, the local dopant concentration in the domains could increase to 40 at. % or higher, and then the value of P_{VO} increases to about 2 or larger. In this case, the oxygen vacancies are easily connected and then the local ordering could further form in the domains.

Although the dopant segregation, and thereby the enrichment of associated oxygen vacancies, can be of benefit to the local ordering of oxygen vacancies, the experimental result showed that a higher degree of ordering is most likely to form in Sm- and Gd-doped ceria instead of in Yb-doped ceria, which has a higher association enthalpy. This fact indicates that there are a variety of factors that could influence the ordering of oxygen vacancies. Since the superstructure of
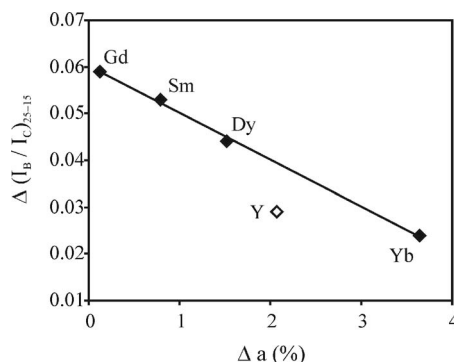

FIG. 10. Values of $\Delta(I_B/I_C)_{25-15}$ as a function of the mismatch between lattice parameters of C-type Ln_2O_3 and fluorite-structured ceria (Δa). The data of Y-doped ceria are also displayed for comparison.

oxygen-vacancy ordering can be approximately described between ceria and Ln_2O_3, we suspect that another influencing factor for the formation ability of the ordering could be the lattice difference between the fluorite-structured ceria and C-type Ln_2O_3. For this reason, the mismatch between lattice parameters of CeO_2 and C-type Ln_2O_3 was calculated as $\Delta a = |1/2 a_C - a_F|/a_F$, where a_F and a_C are the lattice parameters of fluorite-structured CeO_2 and C-type Ln_2O_3.[32] Figure 10 presents the values of $\Delta(I_B/I_C)_{25-15}$ of Ln-doped ceria as a linear function of Δa, clearly showing that the lattice mismatch between the fluorite matrix and the target structure of the ordering may provide resistance to the transition of oxygen-vacancy arrangement from a random distribution in ceria to a more ordered status as in C-type Ln_2O_3 and, thereby, a smaller value of Δa facilitates the formation of oxygen-vacancy ordering in nanosized domains. In a previous study,[17] the relationship between Δa and the dopant dependence of oxygen-vacancy ordering in some heavily doped ceria was also discussed though the correlation was not as clear as in this study. In that work, however, the ordering was examined by comparing heavily doped ceria with pure ceria, which may induce extra errors to the calculation because the defect structures in practical pure ceria (CeO_{2-x}) (Ref. 33) could be complex and quite different from those in rare-earth-doped ceria. In the present work, this deficiency has been overcome with estimating the tendency of ordering by the comparison between samples with different doping levels. Besides the lattice difference, other physical properties of the dopant, e.g., the electronic configuration, may also have impact on the formation of local ordering. In Fig. 10, the data for Y-doped ceria are also displayed for comparison, of which Y has a quite different electronic configuration from those of lanthanides ($Y^{3+}:[Kr]4d^0$; $Ln^{3+}:[Xe]4f^n$, $n=0-14$). Probably because of this, a deviation of this material from the linear correlation belonging to Ln-doped ceria can be readily seen though the radius of Y^{3+} cation[34] and the value of Δa are similar to those of the lanthanides.

According to above discussions, there could be two ways to control the oxygen-vacancy ordering in doped ceria, and thus improve the ionic conduction in ceria-based electrolytes. Firstly, one can carefully select one or more dopants

that can lead to a larger value of Δa but maintain a smaller association enthalpy. Another way is to control the dopant segregation by adjusting parameters in the process of electrolyte preparation. Since the second method can limit both the ordering of oxygen vacancies and the strong interaction between oxygen vacancies and segregated dopant cations, it may lead to a notable improvement in the electrical properties, which has been proved to be promising in Yb- and Y-doped ceria.[10,11]

VI. CONCLUSION

Comparative studies of EELS and SAED have clearly shown the relationship of the local ordering of oxygen vacancies, the doping concentration, the dopant type, and the ionic conductivity in Ln-doped ceria (Ln=Sm, Gd, Dy, and Yb). An increase in the local ordering is observed with increasing the doping concentration and a dependence on dopant type in the sequence of $(Gd, Sm) > Dy > Yb$ can be noticed in the samples with different doping levels. In addition to the interaction between oxygen vacancies and segregated dopant cations, the oxygen-vacancy ordering can further decrease the mobility of oxygen vacancies and then lead to a lower ionic conductivity. Based on the SAED study, a super-structure is constructed for the oxygen-vacancy ordering in Ln-doped ceria, in which the arrangement of oxygen vacancies is similar to those in C-type Ln_2O_3 and $\frac{1}{2}\langle 110 \rangle$ and $\frac{1}{2}\langle 111 \rangle$ pairs are allowed as basic connections of the local ordered structure. It is suggested that the segregation of dopant cations in nanosized domains plays an important role in the local ordering of oxygen vacancies in doped ceria. Furthermore, the ability to form the oxygen-vacancy ordering can be influenced by the association between oxygen vacancies and segregated dopant cations, the lattice mismatch between fluorite-structured ceria and C-type Ln_2O_3 oxides, and physical properties of the dopant such as the electronic configuration.

ACKNOWLEDGMENTS

*Corresponding author; dingrong.ou@nims.go.jp

[1] B. C. H. Steele and A. Heinzel, Nature (London) **414**, 345 (2001).

[2] H. Inaba and H. Tagawa, Solid State Ionics **83**, 1 (1996).

[3] G. B. Balazs and R. S. Glass, Solid State Ionics **76**, 155 (1995).

[4] K. Eguchi, T. Setoguchi, T. Inoue, and H. Arai, Solid State Ionics **52**, 165 (1992).

[5] E. C. Subbarao and H. S. Maiti, Solid State Ionics **11**, 317 (1984).

[6] V. Butler, C. R. A. Catlow, B. E. F. Fender, and J. H. Harding, Solid State Ionics **8**, 109 (1983).

[7] R. Gerhardt-Anderson and A. S. Nowick, Solid State Ionics **5**, 547 (1981).

[8] T. Mori, J. Drennan, J.-H. Lee, J.-G. Li, and T. Ikegami, Solid State Ionics **154-155**, 461 (2002).

[9] T. Mori, J. Drennan, Y. Wang, G. Auchterlonie, J.-G. Li, and A. Yago, Sci. Technol. Adv. Mater. **4**, 213 (2003).

[10] F. Ye, T. Mori, D. R. Ou, M. Takahashi, J. Zou, and J. Drennan, J. Electrochem. Soc. **154**, B180 (2007).

[11] D. R. Ou, T. Mori, F. Ye, M. Takahashi, J. Zou, and J. Drennan, Acta Mater. **54**, 3737 (2006).

[12] D. R. Ou, T. Mori, F. Ye, J. Zou, G. Auchterlonie, and J. Drennan, Electrochem. Solid-State Lett. **10**, P1 (2007).

[13] T. S. Zhang, J. Ma, L. B. Kong, S. H. Chan, and J. A. Kilner, Solid State Ionics **170**, 209 (2004).

[14] T. R. Welberry, B. D. Butler, J. G. Thompson, and R. L. Withers, J. Solid State Chem. **106**, 461 (1993).

[15] S. García-Martín, M. A. Alario-Franco, D. P. Fagg, A. J. Feighery, and J. T. S. Irvine, Chem. Mater. **12**, 1729 (2000).

[16] A. Gallardo-López, J. Martínez-Fernández, A. Domínguez-Rodríguez, and F. Ernst, Philos. Mag. A **81**, 1675 (2001).

[17] D. R. Ou, T. Mori, F. Ye, J. Zou, G. Auchterlonie, and J. Drennan, Appl. Phys. Lett. **89**, 171911 (2006).

[18] A. Travlos, N. Boukos, G. Apostolopoulos, and A. Dimoulas, Appl. Phys. Lett. **82**, 4053 (2003).

[19] R. F. Klie, Y. Ito, S. Stemmer, and N. D. Browning, Ultramicroscopy **86**, 289 (2001).

[20] M. I. Mendelson, J. Am. Ceram. Soc. **52**, 433 (1969).

[21] L. A. J. Garvie and P. R. Buseck, J. Phys. Chem. Solids **60**, 1943 (1999).

[22] R. F. Egerton, *Electron Energy Loss Spectroscopy in the Electron Microscope*, 2nd ed. (Plenum, New York, 1996).

[23] R. C. Karnatak, J. Alloys Compd. **192**, 64 (1993).

[24] L. Douillard, M. Gautier, N. Thromat, M. Henriot, M. J. Guittet, J. P. Duraud, and G. Tourillon, Phys. Rev. B **49**, 16171 (1994).

[25] A. V. Soldatov, T. S. Ivanchenko, S. Della Longa, A. Kotani, Y. Iwamoto, and A. Bianconi, Phys. Rev. B **50**, 5074 (1994).

[26] J. A. Rodriguez, J. C. Hanson, J.-Y. Kim, G. Liu, A. Iglesias-Juez, and M. Fernández-García, J. Phys. Chem. B **107**, 3535 (2003).

[27] J. Yuan, T. Hirayama, Y. Ikuhara, and T. Sakuma, Micron **30**, 141 (1999).

[28] S. Arai, S. Muto, J. Murai, T. Sasaki, Y. Ukyo, K. Kuroda, and H. Saka, Mater. Trans., JIM **45**, 2951 (2004).

[29] J. A. Kilner and B. C. H. Steele, in *Nonstoichiometric Oxides*, edited by O. T. Sørensen (Academic, New York, 1981), pp. 234-237.

[30] V. Longo and L. Podda, J. Mater. Sci. **16**, 839 (1981).

[31] D. J. M. Bevan and E. Summerville, in *Handbook on the Physics and Chemistry on Rare Earths*, edited by K. A. Gschneidner and L. R. Eyring (North-Holland, Amsterdam, 1979), Vol. 3.

[32] JCPDS-International Center for Diffraction Data Card No. 43-1002; Card No. 43-1006; Card No. 43-1014; Card No. 43-1029; Card No. 43-1037.

[33] O. T. Sørensen, in *Nonstoichiometric Oxides*, edited by O. T. Sørensen (Academic, New York, 1981), pp. 15–28.

[34] R. D. Shannon and C. T. Prewitt, Acta Crystallogr., Sect. B: Struct. Crystallogr. Cryst. Chem. **B25**, 925 (1969).